Title

Enhanced Stratospheric Water Vapor over the Summertime Continental United States and the Role of Overshooting Convection

Robert L. Herman[1], Eric A. Ray[2], Karen H. Rosenlof[2], Kristopher M. Bedka[3], Michael J. Schwartz[1], William G. Read[1], Robert F. Troy[1], Keith Chin[1], Lance E. Christensen[1], Dejian Fu[1], Robert A. Stachnik[1], T. Paul Bui[4], Jonathan M. Dean-Day[5]

[1]Jet Propulsion Laboratory, California Institute of Technology, Pasadena, California, USA.

[2]National Oceanic and Atmospheric Administration (NOAA) Earth System Research Laboratory (ESRL) Chemical Sciences Division, Boulder, Colorado, USA.

[3]NASA Langley Research Center, Hampton, Virginia, USA.

[4]NASA Ames Research Center, Moffett Field, California, USA.

[5]Bay Area Environmental Research Institute, Sonoma, California, USA.

Correspondence to: R. L. Herman (Robert.L.Herman@jpl.nasa.gov)

Abstract

The NASA ER-2 aircraft sampled the lower stratosphere over North America during the NASA Studies of Emissions and Atmospheric Composition, Clouds and Climate Coupling by Regional Surveys (SEAC^{4}RS) field mission. This study reports observations of convectively-influenced air parcels with enhanced water vapor in the overworld stratosphere over the summertime continental United States, and investigates in detail three case studies. Water vapor mixing ratios greater than 10 ppmv, much higher than the background 4 to 6 ppmv of the overworld stratosphere, were measured by the JPL Laser Hygrometer (JLH Mark2) at altitudes between 16.0 and 17.5 km (potential temperatures of approximately 380 K to 410 K). Overshooting cloud tops (OT) are identified from a SEAC^{4}RS OT detection product based on satellite infrared window-channel brightness-temperature gradients. Through trajectory analysis, we make the connection between these *in situ* water measurements and OT. Back trajectory analysis ties enhanced water to OT one to seven days prior to the intercept by the aircraft. The trajectory paths are dominated by the North American Monsoon (NAM) anticyclonic circulation. This connection suggests that ice is convectively transported to the overworld stratosphere in OT events and subsequently sublimated; such events may irreversibly enhance stratospheric water vapor in the summer over Mexico and the United States. Regional context is provided by water observations from the Aura Microwave Limb Sounder (MLS).

Keywords

Convection, overshoot, atmospheric water, stratosphere-troposphere exchange

Copyright Statement

Copyright 2017. All rights reserved.

1. Introduction

Water plays a predominant role in the radiative balance of the Earth's atmosphere, both in the gas phase as the Earth's primary greenhouse gas and in condensed phases in cloud and aerosol. Despite its low abundance, upper tropospheric and lower stratospheric (UTLS) water vapor is critically important in controlling outgoing long-wave radiation, and quantifying UTLS water vapor and its controlling processes is critical for climate characterization and prediction. Climate models are sensitive to changes in stratospheric water (Shindell, 2001) and clouds (Boucher et al., 2013). Increases in UTLS water are associated with warming at the surface on the decadal scale (Solomon et al., 2010). As the dominant source of hydroxyl radicals, UTLS water also plays an important role in control of UTLS ozone (Shindell, 2001; Kirk-Davidoff et al., 1999).

The overworld stratosphere, the altitude region with potential temperature θ greater than 380 K (Holton et al. 1995), is extremely dry, with typical mixing ratios of 3—6 parts per million by volume (ppmv). The importance of low temperatures at the tropical tropopause acting as a "cold trap" to prevent tropospheric water from entering the stratosphere has been recognized since Brewer (1949). Tropospheric air slowly ascends through the tropical tropopause layer (TTL) as part of the hemispheric-scale Brewer-Dobson circulation. In the TTL, air passes through extremely cold regions where water vapor condenses in situ to form cirrus ice, and then the cirrus slowly falls due to sedimentation (e.g., Jensen et al., 2013). Additional condensation and sedimentation are thought to be associated with convection and large-scale waves (e.g., Voemel et al., 2002). The amount of water that enters the stratosphere is largely a function of the coldest temperature a parcel trajectory encounters. This typically occurs in the tropics, and the coldest temperature is typically near the tropical tropopause. The saturation mixing ratio at the cold point tropopause thereby sets the entry value of water vapor.

In contrast to water entry into the overworld stratosphere, water transport from the troposphere to the lowermost stratosphere ($350\ \text{K} < \theta < 380\ \text{K}$ over summer CONUS) may occur through several different pathways. Poleward of the subtropical jet, water may be transported into the lowermost stratosphere through isentropic troposphere-stratosphere exchange (Holton et al., 1995) or through convective overshoot of the local tropopause (Dessler et al., 2007; Hanisco et al., 2007). Isentropic transport from the tropics is the dominant pathway for water into the lowermost stratosphere, with evidence from the seasonal cycle of lower stratospheric water (e.g., Flury et al., 2013). How important sublimation of ice from convective overshoot is for hydrating the stratosphere is a topic of ongoing debate (e.g., Randel et al., 2015; Wang, 2003). Case studies have reported extreme events in which ice is transported to the overworld stratosphere and subsequently sublimates, but the amount of ice that is irreversibly injected into the stratosphere is poorly known. Airborne measurements have demonstrated that convective injection occurs both in the tropics (Webster and Heymsfield, 2003; Corti et al., 2008; Sayres et al., 2010; Sargent et al., 2014) and at mid-latitudes (Hanisco et al., 2007; Anderson et al., 2012). Ice injected directly into the stratosphere is unaffected by the cold trap in the vicinity of the tropopause (Ravishankara, 2012).

The subject of this paper is the role of convective overshooting tops in enhancing stratospheric water. Paraphrasing Bedka et al. (2010), a convective overshooting top (OT) is a protrusion above a cumulonimbus anvil due to strong

updrafts above the equilibrium level. Early observations of OT include photographs of OT in the stratosphere from a U-2 aircraft (Roach 1967). Recent observations of elevated water mixing ratios in the summer overworld stratosphere by aircraft (Anderson et al., 2012) and the Aura Microwave Limb Sounder (MLS) (Schwartz et al., 2013) suggest that ice injection into the overworld stratosphere by OT, while rare, occurs in three predominant regions during the summer season. These three regions are the Asian Monsoon region, the South American continent, and – the focus of this study - the North American Monsoon (NAM) region (Schwartz et al., 2013).

The NASA ER-2 aircraft sampled the summer stratospheric NAM region during the NASA Studies of Emissions and Atmospheric Composition, Clouds and Climate Coupling by Regional Surveys (SEAC^{4}RS) field mission (Toon et al., 2016). One of the primary goals of this multi-aircraft mission was to address the question: do deep convective cloud systems locally inject water vapor and other chemicals into the overworld stratosphere over the continental United States (CONUS)? It is challenging for space- and ground-based techniques to detect enhanced water vapor injected into the stratosphere by OT. Satellite measurements are limited by their horizontal and vertical resolution in detecting fine-scale three-dimensional variations in water vapor, while ground-based measurements are confined to sampling at fixed locations. In contrast, airborne *in situ* stratospheric measurements of water have an advantage because the aircraft can be routed to a specific location, altitude, date and time. Modelers can predict whether air parcels are likely to have convective influence, and aircraft flight paths are planned to intercept those air parcels. The purpose of this paper is to report three new case studies of enhanced water vapor in the overworld stratosphere during the NASA SEAC^{4}RS field mission, and to connect these observations to deep convective OT over the North American continent.

2. Observations

2.1 Aircraft

The airborne *in situ* water vapor measurements reported here are from the Jet Propulsion Laboratory Laser Hygrometer Mark2 (JLH Mark2), a tunable laser spectrometer with an open-path cell external to the aircraft fuselage (May, 1998). Water vapor is reported at 1 Hz (10% accuracy), although the time response of the open-path cell is much faster than this because the instrument is sampling the free-stream airflow. This instrument has a redesigned optomechanical structure for greater optical stability, and was first flown in this configuration on the NASA ER-2 high-altitude aircraft during the SEAC^{4}RS field mission. Pressure and temperature, provided by the Meteorological Measurement System (MMS) (Scott et al., 1990), are used in the data processing to calculate water vapor mixing ratios from spectra, as described in May (1998).

During SEAC^{4}RS, nine aircraft flights targeted air parcels with recent convective influence (see Table 3 of Toon et al., 2016). Figure 1 shows the combined vertical profiles of JLH Mark2 water vapor from all 23 SEAC^{4}RS flights. Outliers with high water vapor mixing ratios are the focus on this study. Enhanced water vapor was measured on eleven flights (Table 1). Here we define ‘enhanced water vapor’ as mixing ratios greater than two standard deviations above the mean in situ measurement. For the overworld stratosphere in all 23 SEAC^{4}RS flights, mean

H_2O is 6.7±1.5 ppmv at 380-400 K and 5.0±0.8 ppmv at 400-420 K (Figure 2). Thus, the threshold for enhanced water vapor is 9.7 ppmv at 380-400 K, and 6.6 ppmv at 400-420 K. The majority of measurements have background water mixing ratios characteristic of the overworld stratosphere, 4 to 6 ppmv. In the overworld stratosphere (potential temperature greater than 380 K), Figure 1 shows enhanced water vapor at potential temperatures up to approximately 410 K (17.5 km altitude). We define the 'enhanced water region' as the layer of the overworld stratosphere where these events have been observed, 380-410 K potential temperature corresponding to 16-17.5 km altitude. Enhanced water vapor measured *in situ* by both the JLH Mark2 instrument (Figure 1) and the Harvard Water Vapor instrument (J. B. Smith, pers. comm.) on the NASA ER-2 aircraft indicated that the aircraft intercepted convectively-influenced air. Other tracers measured on the aircraft did not change significantly in these plumes. For the SEAC^{4}RS flights, the agreement between these two water vapor instruments is within +/-10% for stratospheric water. This is consistent with the AquaVIT laboratory intercomparison (Fahey et al., 2014) and other aircraft field missions (e.g., Rollins et al., 2014). The largest enhancements were observed on three flights that are described in detail in Sect. 4.

2.2 Aura MLS

Aura MLS measures ~3500 profiles each day of water vapor and other atmospheric species (Livesey et al., 2016). While the aircraft samples *in situ* water in a thin trajectory through the atmosphere, Aura MLS provides a larger scale context. Expanding on the analysis of Schwartz et al. (2013), Aura MLS observations of stratospheric water vapor are presented here for the SEAC^{4}RS time period of summer 2013. Aura MLS H_2O has 0.4 ppmv precision at 100 hPa for individual profile measurements, with spatial representativeness of 200 km along line-of-sight (Schwartz et al., 2013). Results shown here use MLS version 4.2 data, but are not significantly different from the previous version 3.3. MLS observations over CONUS are at ~14:10 local time (ascending orbit) and~1:20 local time (descending orbit), with successive swaths separated by ~1650 km. Vertical resolution of the water vapor product is ~3 km in the lower stratosphere (Livesey et al., 2016).

Aura MLS shows a seasonal maximum in water vapor over CONUS in July and August. The histogram of Aura MLS water vapor in Figure 3 indicates that the July-August 2013 CONUS lower stratosphere was drier than the previous nine-summer MLS record (2004 to 2012). Nevertheless, enhanced lower stratospheric water vapor was observed by MLS in 2013 as rare but detectable events. From the MLS histogram, the frequency of 100-hPa H_2O > 8ppmv was 0.9% of the observations in July-August 2013 in the blue shaded box. Figure 4 shows that, out of all MLS 100-hPa water vapor retrievals over the two-month period July to August 2013, water greater than 8 ppmv was measured only nine times over North America (in the blue shaded box), three times near the west coast of Mexico, and once over the Caribbean Sea.

3. Analysis

Here we briefly describe the analytical technique used to determine whether back trajectories from the aircraft location intersect OT as identified by a satellite OT data product.

3.1 Detection of overshooting tops

In order to link the stratospheric water vapor encountered by the aircraft to the storm systems from which they may have originated, it is necessary to have a comprehensive continental scale catalog of deep convection. Geostationary Operational Environmental Satellite (GOES) infrared imagery is used to assemble a catalog of OTs throughout the U.S. and offshore waters. This catalog was acquired from the NASA LaRC Airborne Science Data for Atmospheric Composition data archive (http://www-air.larc.nasa.gov/cgi-bin/ArcView/seac4rs). Because OTs are correlated with storm intensity, the OT product was primarily developed to benefit the aviation community for more accurate turbulence prediction, as well as the general public for earlier severe storm warnings. However, the product is also ideally suited for identifying storm systems that can moisten the stratosphere.

Infrared brightness temperatures are used to detect cloud top temperature anomalies within thunderstorm anvils. OT candidates are colder than the mean surrounding anvil, with the temperature difference indicative of both the strength of the convective updraft and the depth of penetration. For a description of the method, the reader is directed to Bedka et al. (2010). The horizontal spatial resolution of the OT product is dependent on the underlying satellite imagery resolution, i.e., the size of the GOES IR pixel, which is 7 km or less over the CONUS. Additional validation of OTs requires comparison with the Global Forecast System (GFS) Numerical Weather Prediction (NWP) model tropopause temperature. The maximum OT cloud height was derived based on knowledge of the 1) OT-anvil temperature difference, 2) the anvil cloud height based on a match of the anvil mean temperature near to the OT and the GFS NWP temperature profile, and 3) a temperature lapse rate within the UTLS region based on a GOES-derived OT-anvil temperature difference and NASA CloudSat OT-anvil height difference for a sample of direct CloudSat OT overpasses (Griffin et al., 2016). Griffin et al. (2016) finds that 75% of OT height retrievals are within 0.5 km of CloudSat OT height, so we conservatively estimate the accuracy of the OT altitude to 0.5 km. For SEAC^{4}RS, every available GOES-East and GOES-West scan (typically 15 min resolution) was processed for the full duration of the mission, even for the non-flight days, yielding a detailed and comprehensive picture of the location, timing, and depth of penetration of convective storms over the entire CONUS. The output files include the OT coordinates, time, overshooting intensity in degrees K – which is related to the temperature difference between the OT and the anvil – and an estimate of maximum cloud height for OT pixels in meters.

The ability of GOES-East and GOES-West to observe an OT depends on its lifetime. OTs are transient events with lifetimes typically less than 30 minutes but can exceed an hour in well-organized storms such as mesoscale convective systems and supercell storms (Bedka et al. 2015; Solomon et al., 2016, and references therein). Animations such as the following show the variability of OTs sampled by GOES at 1-min resolution,
Infrared wavelength animation:
http://cimss.ssec.wisc.edu/goes/srsor2015/800x800_AGOES14_B4_MS_AL_IR_animated_2015222_191500_182_2015223_131500_182_IR4AVHRR2.mp4
Visible wavelength animation:

http://cimss.ssec.wisc.edu/goes/blog/wp-content/uploads/2015/08/150811_goes14_visible_srsor_MS_mcs_anim.gif It is clear that some OTs are quite persistent and are both prominent and detectable in IR imagery, but the majority of OTs in these particular animations are short lived (< 10 minutes). Within these OTs, strong convective updrafts can transport ice to 16-18 km altitude where turbulent processes such as gravity wave breaking mix tropospheric and stratospheric air (e.g., Mullendore et al., 2009, 2005; Wang 2003; Homeyer et al. 2017), enabling detrainment of ice and stratospheric hydration.

Bedka et al. (2010) showed that the OT detection algorithm has a false positive rate of 4.2% to 38.8%, depending on the size of the overshooting and algorithm settings. As noted above, OTs are transient and can evolve quite rapidly. The storm top characteristics and evolution we see in the GOES data featured in this paper only capture a subset of the storm lifetimes, even if we were to have a 100% OT detection rate, due to the 15 min resolution of the GOES imager. In addition, relatively coarse GOES spatial resolution (up to 7 km over northern latitudes of the US) can cause the Bedka et al. (2010) method to miss some small diameter and/or weak OT regions. We would be able to better map tracks of storm updrafts using data at 1-minute frequency like that shown by Bedka et al. (2015), but this data is not available over broad geographic domains required for our analysis. Given uncertainties in back trajectories, GOES under-sampling, and that many OTs can be located in close proximity to one another, we are not able to make a direct connection between an individual OT and a stratospheric water vapor plume observed a day or more later. Rather, our analysis identifies a cluster of storms that are the best candidates for generating ice that sublimates into enhanced water vapor plumes sampled by the ER-2.

3.2 Back trajectory modeling

Back trajectories were run from each flight profile where enhanced water vapor was measured to determine whether the sampled air was convectively influenced. The trajectories were run with the FLEXPART model (Stohl et al., 2005) using NCEP Climate Forecast System version 2 (CFSv2) meteorology (Saha et al., 2014), and the trajectory time step interval was one hour. Trajectories were initialized every second along the flight track profiles and run backward for seven days. A sampled air parcel was determined to be convectively influenced if the back trajectory from that parcel intercepted an OT region. The tolerances for a trajectory to be considered to have intercepted an OT cloud were +/-0.25 degrees latitude and longitude, +/-3 hours, +/-0.5 km in altitude. These tolerances were chosen primarily due to the resolution of the NCEP meteorology used to run the trajectories (1 deg x 1 deg) and based on personal communication with Leonard Pfister.

4. Case Studies

In this section, we highlight three NASA ER-2 flights where elevated stratospheric water was observed by JLH Mark2. These dates are 8, 16 and 27 August 2013. Similar results are seen from other hygrometers on the NASA ER-2 aircraft (J. B. Smith, pers. comm.). For each of these ER-2 flights, the back trajectories are presented along with the intersection of coincident OT. The cases are described below.

222 **4.1 First case: 8 August 2013**

223 Figure 5 shows details of the 8 August 2013 ER-2 aircraft flight. This flight was the transit flight from Palmdale,
224 California (34.6 °N, 118.1 °W), to Ellington Field, Houston, Texas (29.6 °N, 95.2 °W). In addition to sending the
225 NASA ER-2 aircraft to the destination base, the science goal of this flight was to profile the North American
226 Monsoon region with five profiles plus the aircraft ascent and final descent. This flight shows a dramatic transition
227 from west to east of background stratospheric water to enhanced water. In the lowermost stratosphere (350 K < θ <
228 380 K), water can be highly variable, but at 90 hPa it is generally unusual to observe water vapor greater than 6
229 ppmv. As shown in Figure 5c, there is a gradient in water vapor from west to east: 4.0 to 4.4 ppmv at 90 hPa (17
230 km) over the west coast of CONUS (black and blue points), and greater than 10 ppmv at 90 hPa over Texas (green
231 points). Simultaneous Aura MLS retrievals also demonstrate a west-to-east water vapor gradient on this day (lines
232 and filled circles in Figure 5c). Both JLH Mark2 and Aura MLS water vapor exceed the thresholds for enhanced
233 water vapor.
234
235 Analysis of the 8 August 2013 case is shown in Figure 6. For clarity only some example trajectories (a subset of our
236 analysis) are shown. These are displayed as thin blue traces in panels (b) and (c). The intersections of the example
237 trajectories with coincident OT are shown as red squares in panels (b) and (c). All overshooting convective tops
238 within +/-3 hours of the red squares are shown by green symbols in panels (b) and (c). Back trajectories from the
239 flight track follow the anticyclonic NAM circulation over Western Mexico, Great Plains and Mississippi Valley
240 (Figure 6b). Every one of the example back trajectories intersects OT, as shown by red symbols in Figure 6b. For
241 this flight, coincidences with overshooting convection are dominated by overshooting clouds over the Mississippi
242 Valley and Great Plains. All overshooting convection within the tolerances prescribed (see Sect. 3.2) for the back
243 trajectories are shown by the green symbols in Figure 6b and 5c. Figure 6c demonstrates the range of altitudes
244 reached by the coincident overshooting convection and how many convective overshooting cells were coincident.
245 The high resolution of the convective overshooting data meant that there could be multiple coincident convective
246 overshooting cells for a single location on a back trajectory. It is significant that some of the green overshooting
247 cells are higher altitude than the red coincident points, suggesting that overshooting air parcels descended slightly
248 before mixing with the surrounding air. Figure 6d indicates the source of enhanced water was dominated by
249 overshooting clouds within seven days prior to intercept by the aircraft.
250
251 **4.2 Second case: 16 August 2013**

252 The NASA ER-2 flight of 16 August 2013 was designed to survey the North American Monsoon in a triangular
253 flight path from Houston, Texas, to the Imperial Valley in Southern California, to Southeastern Colorado and back
254 to Texas. The NASA ER-2 aircraft performed six dives, encountering enhanced stratospheric water at 16 to 17 km
255 altitude (Figure 7a). As shown in Figure 7b, back trajectories intersect overshooting tops over the South Central U.S.
256 (Texas, Oklahoma, Arkansas) and also over the Sierra Madre Occidental mountain range on the west coast of
257 Mexico. This case is an example of the classic North American Monsoon circulation with a moisture source over the
258 Sierra Madre Occidental (Adams and Comrie, 1997), in which air parcels are transported from OT in Mexico,

around the anticyclone, to the CONUS (Figure 7b). The altitude range of the convective overshoot is typically 16 to 17 km altitude, as shown in Figure 7c. The time between OT and intercept by the aircraft ranges from two to seven days (Figure 7d).

4.3 Third case: 27 August 2013

The 27 August 2013 flight performed six dives to sample the North American Monsoon. Stratospheric water was enhanced to 15 to 20 ppmv in altitudes ranging from 16.0 to 17.5 km (Figure 8a). The ER-2 aircraft intercepted highly enhanced stratospheric water from a mesoscale convective complex over the Upper Midwest, which had overshooting tops over Northern Minnesota and Northern Wisconsin (Toon et al., 2016), as shown in Figure 8b. Figure 8c shows an abundance of OT above 17 km (green). Generally speaking, the OT appear at higher altitudes in the northern CONUS/southern Canada than in the Central CONUS. Figure 8d shows that the air masses were sampled *in situ* by the ER-2 aircraft over Illinois and Indiana one to two days after the intense storm. As is a common theme for all these experiment days, a portion of the back-trajectories also trace back to overshooting tops over the Sierra Madre Occidental one week prior.

5. Conclusions

In this paper, we have examined *in situ* measurements of stratospheric water by JLH Mark2 on the ER-2 aircraft during the SEAC^{4}RS field mission. With JLH Mark2 data, enhanced H_2O above background mixing ratios was frequently encountered in the overworld stratosphere between 16 and 17.5 km altitude. Back trajectories initialized at every 1-sec time stamp along the aircraft flight track at 16 to 17.5 km connect the sampled air parcels to convective OT within seven days prior to the flight. The trajectory modeling indicates that the identified OT are associated with larger storm systems over the Central U.S. (Figure 6), deep convection over the Sierra Madre Occidental (Figure 7), and deep convection over the Upper Midwest U.S. and South Central Canada (Figure 8). For all the back trajectories in the three case studies, the fraction that connect to OT within the previous seven days ranges from 30% to 70% (Figure 9). The three aircraft flight dates analyzed in Figure 9 have a higher fraction of enhanced water than the other flights. These three flights deliberately targeted air masses influenced by convection. For the CONUS in general, the fraction of air parcels at 370-420 K influenced by OT is much smaller.

The concentrations of enhanced water and the connection to OT suggests a mechanism for moistening the CONUS lower stratosphere: ice is irreversibly injected into the overworld stratosphere by the most intense convective tops. The temperatures of the CONUS lower stratosphere are sufficiently warm to sublimate the ice, producing water vapor mixing ratios elevated 10 ppmv or more above background levels. The summertime CONUS has a high frequency of thunderstorms with sufficient energy to transport ice to the upper troposphere (Koshak et al., 2015, and references therein). On rare occasion, these storms have sufficient energy to loft ice through the tropopause and into the stratosphere. Further evidence of ice is provided by water isotopologues. Evaporation and condensation are fractionating processes for isotopologues, especially HDO relative to H_2O (e.g., Craig, 1961; Dansgaard, 1964). Condensation preferentially concentrates the heavier HDO isotopologue, so lofted ice is relatively enriched in

296 HDO/H_2O compared to gas phase (e.g., Webster and Heymsfield, 2003, and references therein). Ice sublimation is
297 supported by the enriched HDO/H_2O isotopic signature observed by the ACE satellite over summertime North
298 America (Randel et al., 2010). Cross-tropopause transport is a consequence of turbulent mixing at cloud top,
299 possibly enhanced by the existence of breaking gravity waves often occurring near overshooting cloud tops. (Wang,
300 2003). This study addresses a primary goal of the SEAC^{4}RS field mission (Toon et al., 2016), answering
301 affirmatively the science question: "Do deep convective cloud systems locally inject water vapor and other
302 chemicals into the overworld stratosphere over the CONUS?" This water is almost certainly injected in the ice
303 phase and subsequently sublimated in the relatively warm stratosphere over CONUS, leading to irreversible
304 hydration. From this study, we conclude that the depth of injection was typically 16 to 17.5 km altitude for these
305 particular summertime events.
306
307 Satellite retrievals of water vapor from Aura MLS provide a larger-scale context. The fraction of Aura MLS
308 observations at 100 hPa (approximately 17 km altitude) with H_2O greater than the 8 ppmv threshold is 0.9% for
309 July-August 2013. In comparison, Schwartz et al. (2013) reports that, for the nine-year record 2004-2012, July and
310 August had 1.4% and 3.2% of observations exceed 8 ppmv, respectively. This reinforces the conclusion of Randel et
311 al. (2015) that OT play a minor role in the mid-latitude stratospheric water budget. At the 100-hPa level in the lower
312 stratosphere, the year 2013 was slightly drier than the average of 2004-2012 summers (Figure 3). Despite the
313 relatively dry conditions of summer 2013, there was sufficient enhanced water to be clearly observed in the Aura
314 MLS retrievals (Figures 3, 4, 5). Limb measurements from Aura MLS come from a ~200 km path through the
315 atmosphere with ~3 km vertical resolution in the lower stratosphere (Livesey et al., 2016). The aircraft profiles of
316 water vapor are very similar on ascent and descent profiling (Figure 5c), which allows us to estimate the horizontal
317 length of these features as greater than 180 km, and a vertical thickness of ~0.5 km. This size is sufficiently large
318 that the MLS retrieval is sensitive to enhanced water, as shown in Figure 5c.
319
320 *In situ* measurements probe on a small-scale air parcels that can be connected to OT that inject ice and, to a lesser
321 extent, trace gases to the stratosphere (e.g., Ray et al., 2004; Hanisco et al., 2007; Jost et al, 2004). In contrast,
322 modeling studies tend to focus on large-scale processes. Dessler et al. (2002) and Corti et al. (2008) concluded that
323 OT are a significant source of water vapor in the mid-latitude lower stratosphere. In contrast, Randel et al. (2015)
324 used Aura MLS observations to conclude that circulation plays a larger role than OT in controlling mid-latitude
325 stratospheric water vapor in the NAM monsoon region. Our study shows clear evidence of observable perturbations
326 to stratospheric water vapor on ER-2 aircraft flights that targeted convectively-influenced air during SEAC^{4}RS. In
327 future work, we plan more detailed back trajectory analysis of air parcels over summertime North America to better
328 understand the transport of ice and water in the lower stratosphere.

Code Availability

n/a

Data Availability

Data discussed in this manuscript are publically available. The NASA aircraft data are available through the following digital object identifier (DOI): SEAC4RS DOI 10.5067/Aircraft/SEAC4RS/Aerosol-TraceGas-Cloud.

Appendices: none

Supplement link: none

Team List:

Robert L. Herman[1], Eric A. Ray[2], Karen H. Rosenlof[2], Kristopher M. Bedka[3], Michael J. Schwartz[1], William G. Read[1], Robert F. Troy[1], Keith Chin[1], Lance E. Christensen[1], Dejian Fu[1], Robert A. Stachnik[1], T. Paul Bui[4], Jonathan M. Dean-Day[5]

[1]Jet Propulsion Laboratory, California Institute of Technology, Pasadena, California, USA.

[2]National Oceanic and Atmospheric Administration (NOAA) Earth System Research Laboratory (ESRL) Chemical Sciences Division, Boulder, Colorado, USA.

[3]NASA Langley Research Center, Hampton, Virginia, USA.

[4]NASA Ames Research Center, Moffett Field, California, USA.

[5]Bay Area Environmental Research Institute, Sonoma, California, USA.

Author Contribution

Robert Herman prepared the manuscript with contributions from all coauthors and was responsible for all aspects of the JLH Mark2 as principal investigator. Eric Ray and Karen Rosenlof provided trajectory calculations and interpretation. Kristopher Bedka provided an overshooting top data product and interpretation. Robert Troy, Robert Stachnik and Keith Chin operated the JLH Mark2 instrument in the field and downloaded data. Robert Stachnik, Dejian Fu, Lance Christensen and Keith Chin also developed software components for the JLH Mark2 instrument. Michael Schwartz and William Read provided Aura MLS data and statistical analysis. T. Paul Bui and Jonathan Dean-Day measured pressure and temperature with the MMS instrument and provided data.

Competing interests:

The authors declare that they have no conflict of interest.

Disclaimer

Acknowledgements

We thank Jose Landeros and Dave Natzic for providing technical support in the laboratory and field, and the aircraft crew and flight planners for making these measurements possible. The JLH Mark2 team is supported by the NASA Upper Atmosphere Research Program and Radiation Sciences Program. Part of this research was performed at JPL, California Institute of Technology, under a contract with NASA.

370 **References**

371 Adams, D. K., and A. C. Comrie: The North American Monsoon. *Bull. Amer. Meteor. Soc.*, 78, 2197–2213,
372 doi:http://dx.doi.org/10.1175/JCLI4071.1, 1997.

373 Anderson, J. G., Wilmouth, D. M., Smith, J. B., and Sayres, D. S.: UV Dosage Levels in Summer: Increased Risk
374 of Ozone Loss from Convectively Injected Water Vapor, *Science*, 337(6096), 835-839, 2012.

375 Bedka, K. M., Brunner, J., Dworak, R., Feltz, W., Otkin, J., and Greenwald, T.: Objective satellite-based
376 overshooting top detection using infrared window channel brightness temperature gradients. *J. Appl. Meteor.*
377 *Climatol.*, **49**, 181-202, 2010.

378 Bedka, K. M., Wang, C., Rogers, R., Carey, L., Feltz, W., and Kanak, J.: Examining deep convective cloud
379 evolution using total lightning, WSR-88D, and GOES-14 super rapid scan datasets, *Wea. Forecasting*, 30,
380 571–590, doi:10.1175/WAF-D-14-00062.1, 2015.

381 Boucher, O., Randall, D., Artaxo, P., Bretherton, C., Feingold, G., Forster, P., Kerminen, V.-M., Kondo, Y., Liao,
382 H., Lohmann, U., Rasch, P., Satheesh, S. K., Sherwood, S., Stevens B., and Zhang, X. Y.: Clouds and
383 Aerosols. In: Climate Change 2013: The Physical Science Basis. Contribution of Working Group I to the
384 Fifth Assessment Report of the Intergovernmental Panel on Climate Change (Stocker, T. F., Qin, D., Plattner,
385 G.-K., Tignor, M., Allen, S. K., Boschung, J., Nauels, A., Xia, Y., Bex, V., and Midgley, P. M. (eds.)),
386 Cambridge University Press, Cambridge, United Kingdom and New York, NY, USA, 2013.

387 Brewer, A. W.: Evidence for a world circulation provided by the measurements of helium and water vapor
388 distribution in the stratosphere, *Q. J. Roy. Met. Soc.,* 75, 351-63, 1949.

389 Corti, T., Luo, B. P., De Reus, M., Brunner, D., Cairo, F., Mahoney, M. J., Martucci, G., Matthey, R., Mitev, V.,
390 Dos Sntos, F. H., Schiller, C., Shur, G., Sitnikov, N. M., Spelten, N., Voessing, H. J., Borrmann, S., and
391 Peter, T.: Unprecedented evidence for deep convection hydrating the tropical stratosphere, *Geophys. Res.*
392 *Lett., 35,* L10810, doi:10.1029/2008GL033641, 2008.

393 Craig, H.: Isotopic Variations in Meteoric Waters, *Science, 133,* 1702-3, doi: 10.1126/science.133.3465.1702, 1961.

394 Dansgaard, W.: Stable isotopes in precipitation, *Tellus, 16,* 436-68, 1964.

395 Dessler, A. E., Hanisco, T. F, and Fueglistaler, S.: Effects of convective ice lofting on H_2O and HDO in the tropical
396 tropopause layer, *J. Geophys. Res., 112*, doi:10.1029/2007JD008609, 2007.

397 Fahey, D. W., Gao, R.-S., Möhler, O., Saathoff, H., Schiller, C., Ebert, V., Krämer, M., Peter, T., Amarouche, N.,
398 Avallone, L. M., Bauer, R., Bozóki, Z., Christensen, L. E., Davis, S. M., Durry, G., Dyroff, C., Herman, R.
399 L., Hunsmann, S., Khaykin, S., Mackrodt, P., Meyer, J., Smith, J. B., Spelten, N., Troy, R. F., Vömel, H.,
400 Wagner, S., and Weinhold, F. G.: The AquaVIT-1 Intercomparison of Atmospheric Water Vapor
401 Measurement Techniques, Atmos. Meas. Tech., 7, 3177-3213, doi:10.5194/amt-7-3177-2014, 2014.

402 Flury, T., Wu, D. L., and Read, W. G.: Variability in the speed of the Brewer-Dobson circulation as observed by
403 Aura/MLS, *Atmos. Chem. Phys., 13,* 4563–4575, www.atmos-chem-phys.net/13/4563/2013/,
404 doi:10.5194/acp-13-4563-2013, 2013.

405 Griffin, S. M., Velden, C. S., and Bedka, K. M.: A method for calculating the height of overshooting convective
406 cloud tops using satellite-based IR imager and CloudSat cloud profiling radar observations, J. Appl. Met. and
407 Clim., 55, 479-491, DOI: http://dx.doi.org/10.1175/JAMC-D-15-0170.1, 2016.
408 Hanisco, T. F., Moyer, E. J., Weinstock, E. M., St. Clair, J. M., Sayres, D. S., Smith, J. B., Lockwood, R.,
409 Anderson, J. G., Dessler, A. E., Keutsch, F. N., Spackman, J. R., Read, W. G., and Bui, T. P.: Observations of
410 deep convective influence on stratospheric water vapor and its isotopic composition, *Geophys. Res. Lett., 34,*
411 L04814, doi:10.1029/2006GL027899, 2007.
412 Holton, J.R., P.H. Haynes, A.R. Douglass, R.B. Rood, and L. Pfister: Stratosphere–troposphere exchange. Rev.
413 Geophys., 33(4), 403–439, 1995.
414 Homeyer, C., McAuliffe, J., and Bedka, K. M.: On the Development of Above-Anvil Cirrus Plumes in Extratropical
415 Convection, *J. Atmos. Sci.*, In Press, available online at: http://journals.ametsoc.org/doi/abs/10.1175/JAS-D-
416 16-0269.1
417 Jensen, E. J., Diskin, G., Lawson, R. P., Lance, S., Bui, T. P., Hlavka, D., McGill, M., Pfister, L., Toon, O. B., and
418 Gao, R., Ice nucleation and dehydration in the Tropical Tropopause Layer, Proc. Nat. Acad. Sci., 110(6),
419 2041–2046, 2013.
420 Jensen, E. J., Smith, J. B., Pfister, L., Pittman, J. V., Weinstock, E. M., Sayres, D. S., Herman, R. L., Troy, R. F.,
421 Rosenlof, K., Thompson, T. L., Fridlind, A. M., Hudson, P. K., Cziczo, D. J., Heymsfield, A. J., Schmitt, C.
422 and Wilson, J. C.: Ice Supersaturations Exceeding 100% at the Cold Tropical Tropopause: Implications for
423 Cirrus Formation and Dehydration, Atmos. Chem. Phys., 5, 851-62, 2005.
424 Jost, H. J., et al.: In-situ observations of mid-latitude forest fire plumes deep in the stratosphere, Geophys. Res. Lett.,
425 31, L11101, doi:10.1020/2003GL019253, 2004.
426 Kirk-Davidoff, D. B., Hintsa, E. J., Anderson, J. G., and Keith, D. W.: The effect of climate change on ozone
427 depletion through changes in stratospheric water vapour, *Nature, 402*, 399-401, doi:10.1038/46521, 1999.
428 Koshak, W. J., Cummins, K. L., Buechler, D. E., Vant-Hull B., Blakeslee, R. J., Williams, E. R., and H. S. Peterson:
429 Variability of CONUS Lightning in 2003-12 and Associated Impacts, *J. Appl. Meteor. Climat., 54*, 15-
430 41,doi:10.1175/JAMC-D-14-0072.1, 2015.
431 Livesey, N. J., Read, W. G., Wagner, P. A., Froidevaux, L., Lambert, A., Manney, G. L., Millan Valle, L. F.,
432 Pumphrey, H. C., Santee, M. L., Schwartz, M. J., Wang, S., Fuller, R. A., Jarnot, R. F., Knosp, B. W., and
433 Martinez, E.: Earth Observing System (EOS) Aura Microwave Limb Sounder (MLS) Version 4.2x Level 2
434 data quality and description document, Tech. Rep. JPL D-33509 Rev. B, Version 4.2x-2.0, Jet Propulsion
435 Laboratory, California Institute of Technology, Pasadena, CA, available online at:
436 http://mls.jpl.nasa.gov/data/datadocs.php (last access: May 9, 2016), 2016.
437 Liu, C., Zipser, E. J., Cecil, D. J., Nesbitt, S. W., Sherwood, S.: *J. Appl. Meteorol. Climatol. 47*, 2712: 2008.
438 Liu, N., and Liu, C.: Global distribution of deep convection reaching tropopause in 1 year GPM observations, *J.*
439 *Geophys. Res. Atmos., 121,* doi:10.1002/2015JD024430, 2016.
440 May, R. D.: Open-path, near-infrared tunable diode laser spectrometer for atmospheric measurements of H_2O, J.
441 Geophys. Res., 103(D15), 19161-19172, doi:10.1029/98jd01678, 1998.

Moyer, E., Irion, F., Yung, Y., and Gunson, M.: ATMOS stratospheric deuterated water and implications for troposphere-stratosphere transport, *Geophys. Res. Lett., 23*(17), 2385-88, 1996.

Mullendore, G. L., Durran, D. R., and Holton, J. R.: Cross-tropopause tracer transport in midlatitude convection, *J. Geophys. Res., 110,* D06113, doi:10.1029/2004JD005059, 2005.

Mullendore, G. L., Homann, A. J., Bevers, K., and Schumacher, C.: Radar reflectivity as a proxy for convective mass transport*, J. Geophys. Res., 114,* D16103, doi:10.1029/2008JD011431, 2009.

Randel, W. J., K. Zhang, and R. Fu: What controls stratospheric water vapor in the NH summer monsoon regions?, *J. Geophys. Res.*, 120, 7988–8001, doi:10.1002/2015JD023622, 2015.

Ravishankara, A. R.: Water Vapor in the Lower Stratosphere, Science, 337, 809–810, doi: 10.1126/science.1227004, 2012.

Ray, E. A., Rosenlof, K. H., Richard, E. C., Hudson, P. K., Cziczo, D. J., Loewenstein, M., Jost, H.-J., Lopez, J., Ridley, B., Weinheimer, A., Montzka, D., Knapp, D., Wofsy, S. C., Daube, B. C., Gerbig, C., Xueref, I., and Herman, R. L.: Evidence of the effect of summertime midlatitude convection on the subtropical lower stratosphere from CRYSTAL-FACE tracer measurements, J. Geophys. Res., 109(D18), D18304, doi: 10.1029/2004JD004655, 2004.

Read, W. G., et al.: Aura Microwave Limb Sounder upper tropospheric and lower stratospheric H_2O and relative humidity with respect to ice validation, J. Geophys. Res. Atmospheres, 112(D24), D24S35, doi:10.1029/2007jd008752, 2007.

Roach, W. T.: On the nature of the summit areas of severe storms in Oklahoma, *Q. J. R. Meteorol. Soc., 93*, 318–336, 1967.

Rodgers, C. D.: Inverse Methods for Atmospheric Sounding: Theory and Practice, World Science, London, 2000.

Rodgers, C. D., and Connor, B. J.: Intercomparison of Remote Sounding Instruments, J. Geophys. Res., 108, 4116, doi: 10.1029/2002JD002299, 2003.

Rollins, A., Thornberry, T., Gao, R. S., Smith, J. B., Sayres, D. S., Sargent, M. R., Schiller, C., Krämer, M., Spelten, N., Hurst, D. F., Jordan, A. F., Hall, E. G., Vömel, H., Diskin, G. S., Podolske, J. R., Christensen, L. E., Rosenlof, K. H., Jensen, E. J., and Fahey, D. W.: Evaluation of UT/LS hygrometer accuracy by inter-comparison during the NASA MACPEX mission, J. Geophys. Res.-Atmos., 119, doi:10.1002/2013JD020817, 2014.

Saha, S. et al.: The NCEP Climate Forecast System Version 2, J. Climate, 27, 2185–2208, doi:10.1175/JCLI-D-12-00823.1, 2014.

Sargent, M. R., Smith, J. B., Sayres, D. S., and Anderson, J. G.: The roles of deep convection and extratropical mixing in the Tropical Tropopause Layer: An in situ measurement perspective, *J. Geophys. Res., 119*(21), 12355-71, DOI:10.1002/2014JD022157, 2014.

Sayres, D. S., Pfister, L., Hanisco, T. F., Moyer, E. J., Smith, J. B., St. Clair, J. M., O'Brien, A. S., Witinski, M. F., Legg, M., and Anderson, J. G.: Influence of convection on the water isotopic composition of the tropical tropopause layer and tropical stratosphere, *J. Geophys. Res., 115,* D00J20, doi:10.1029/2009JD013100, 2010.

Schwartz, M. J., Read, W. G., Santee, M. L., Livesey, N. J., Froidevaux, L., Lambert, A., and Manney, G. L.: Convectively injected water vapor in the North American summer lowermost stratosphere, Geophys. Res. Lett., 40, 2316-2321, doi:10.1002/grl.50421, 2013.

Scott, S. G., Bui, T. P., Chan, K. R., and Bowen, S. W.: The meteorological measurement system on the NASA ER-2 aircraft, J. Atmos. Ocean. Tech., 7, 525-40, 1990.

Shindell, D. T.: Climate and ozone response to increased stratospheric water vapor, *Geophys. Res. Lett., 28,* 1551-4, 2001.

Smith, J. B., Sargent, M., Wilmouth, D. and Anderson, J. G.: Quantifying the Direct Convective Transport of Tropospheric Air to the Overworld Statosphere, Abstract A51O-0288, presented at 2015, Fall Meeting, AGU, San Francisco, CA, 14-18 December, 2015.

Solomon, D. L., Bowman, K. P., and Homeyer, C. R.: Tropopause-Penetrating Convection from Three-Dimensional Gridded NEXRAD Data, *J. Appl. Met. Climat., 55,* 465-78, DOI:10.1175/JAMC-D-15-0190.1, 2016.

Solomon, S., Rosenlof, K. H., Portmann, R. W., Daniel, J. S., Davis, S. M., Sanford, T. J., and Plattner, G.-K.: Contributions of Stratospheric Water Vapor to Decadal Changes in the Rate of Global Warming, Science, 327(5970), 1219-1223, doi:10.1126/science.1182488, 2010.

Stohl, A., C. Forster, A. Frank, P. Seibert, and G. Wotawa: Technical note: The Lagrangian particle dispersion model FLEXPART version 6.2, Atmos. Chem. Phys., 5, 2461-2474, doi: 10.5194/acp-5-2461-2005-supplement, 2005.

Toon, O. B., H. Maring, J. Dibb, R. Ferrare, D. J. Jacob, E. J. Jensen, Z. J. Luo, G. G. Mace, L. L. Pan, L. Pfister, K. H. Rosenlof, J. Redemann, J. S. Reid, H. B. Singh, A. M. Thompson, R. Yokelson, P. Minnis, G. Chen, K. W. Jucks, and A. Pszenny: Planning, implementation and scientific goals of the Studies of Emissions and Atmospheric Composition, Clouds and Climate Coupling by Regional Surveys (SEAC^{4}RS) field mission, *J. Geophys. Res., 121*, 4967-5009, doi:10.1002/2015JD024297, 2016.

Voemel, H., et al.: Balloon-borne observations of water vapor and ozone in the tropical upper troposphere and lower stratosphere, *J. Geophys. Res.*, 107(D14), pages ACL 8-1-ACL 8-16, DOI:10.1029/2001JD000707, 2002. Available online at http://onlinelibrary.wiley.com/doi/10.1029/2001JD000707/full#jgrd8979-fig-0017, 2002.

Wang, P. K., Moisture plumes above thunderstorm anvils and their contributions to cross-tropopause transport of water vapor in midlatitudes, *J. Geophys. Res., 108*(D6), 4194, doi:10.1029/2002JD002581, 2003.

Webster, C. R., and Heymsfield, A. J.: Water Isotope Ratios D/H, $^{18}O/^{16}O$, $^{17}O/^{16}O$ in and out of Clouds Map Dehydration Pathways, *Science*, 302, 1742, DOI: 10.1126/science.1089496, 2003.

TABLES

Table 1 Summary of enhanced water vapor measurements in the overworld stratosphere during SEAC^{4}RS*. Dates are NASA ER-2 aircraft flight dates in day-month-year format, and JLH Mark2 maximum water vapor mixing ratios (ppmv) are shown for potential temperatures greater than 400 K (left) and in the range 380-400 K (right).

Date	max. water (ppmv)	Pot. Temp. (K)	Altitude (km)	max. water (ppmv)	Pot. Temp. (K)	Altitude (km)
	above 400 K	above 400 K	above 400 K	380-400K	380-400K	380-400K
8-Aug-2013	10.1	401.2	17.29	11.2	385.7	17.10
12-Aug-2013	8.0	400.1	17.08	13.2	388.1	16.86
14-Aug-2013	7.7	402.2	17.38	10.7	387.4	16.75
16-Aug-2013	7.0	400.2	17.14	12.2	387.3	16.82
27-Aug-2013	15.3	402.8	17.32	17.7	380.8	16.12
30-Aug-2013	9.2	400.2	17.27	12.0	390.0	16.81
2-Sep-2013	8.0	400.3	17.07	13.0	380.3	16.28
4-Sep-2013	6.3	405.0	17.57	10.8	380.2	16.32
6-Sep-2013	6.8	400.1	17.12	15.6	381.0	16.32
11-Sep-2013	7.7	400.2	17.13	10.2	381.0	16.22
13-Sep-2013	6.9	401.8	17.55	9.2	382.4	16.41

* SEAC^{4}RS = Studies of Emissions and Atmospheric Composition, Clouds and Climate Coupling by Regional Surveys

FIGURE CAPTIONS

Figure 1. JLH Mark2 stratospheric water vapor profiles from 23 aircraft flights during SEAC^{4}RS. This altitude range includes the overworld stratosphere (potential temperature greater than 380 K) and lowermost stratosphere (tropopause to 380 K). The majority of observations have mixing ratios less than 10 ppmv in the lowermost stratosphere and less than 6 ppmv in the overworld stratosphere. Enhanced water measurements are the extreme outliers with high water mixing ratios, with a threshold value of mean plus two standard deviations.

Figure 2. Distribution of JLH Mark2 water vapor in the overworld stratosphere for all flights in the SEAC^{4}RS mission (summer 2013), plotted as fraction of observations in each potential temperature range. First trace (black circles and line) is at potential temperatures 380 K to 400 K corresponding to approximately 16.8 to 17.4 km altitude (99 to 90 hPa). Second trace (red triangles and line) is at potential temperatures 400 to 420 K corresponding to approximately 17.4 to 18.0 km altitude (90 to 80 hPa).

Figure 3. Distribution of Aura MLS v4.2 100-hPa H_2O over CONUS (blue shaded box in insert), corresponding to approximately 17 km altitude. The two histograms for July-August 2013 (blue asterisks and trace) and the previous nine-summer MLS record, July-August 2004 through 2012 (red circles and trace) indicates that 2013 was drier than average. The threshold for MLS-detected 'enhanced water vapor' (thick black vertical line) is set at 8 ppmv, same as Schwartz et al. (2013), to exclude the larger population of measurements at 6 to 8 ppmv water vapor that may have other sources.

538 **Figure 4.** Two-month mean map of Aura MLS v4.2 100-hPa H_2O (color scale), corresponding to approximately 17
539 km altitude, with superimposed MERRA horizontal winds (arrows) for July-August 2013 during the SEAC^{4}RS time
540 period. MLS observations of 100-hPa H_2O greater than 8 ppmv in this two-month period are shown by the white
541 circles.
542
543 **Figure 5.** Map and profiles of aircraft and satellite water vapor on 8 August 2013 over California (number 1 shown
544 in dark blue) and Texas (number 2 shown in green). (a) Map of ER-2 aircraft flight track (solid colored trace) and
545 nearly coincident Aura MLS geolocations (asterisks and lines). (b) ER-2 aircraft altitude profiles (solid colored
546 trace) color-coded by dives and MLS times (horizontal lines). (c) Vertical profiles of *in situ* water vapor
547 measurements from JLH Mark2 (dots) and MLS retrievals of water vapor (circles and lines). Some measurements
548 exceed the threshold for enhanced water vapor of 8 ppmv for Aura MLS (after Schwartz et al., 2013), and the
549 campaign-wide mean plus 2 st. dev. for JLH Mark 2, 9.7 ppmv at 380-400 K and 6.6 ppmv at 400-420 K.
550
551 **Figure 6.** Analysis of the 8 August 2013 NASA ER-2 aircraft flight. (a) Vertical profiles of JLH Mark2 *in situ* H_2O.
552 Back trajectories were initialized from all aircraft water measurements at 16 to 17.5 km altitude. (b) Example back
553 trajectories (thin blue traces) and coincident overshooting convection (red). Along the NASA ER-2 flight track
554 (orange line), enhanced water vapor was measured (thick blue lines). This figure identifies where trajectories and
555 OT are coincident (red squares) within tolerances prescribed in Section 3.2. The green markers are overshooting
556 convective tops within +/-3 hours of the red squares to indicate the main regions of convective overshooting during
557 the seven days prior to the ER-2 flight and which of those regions appeared to contribute most to the water vapor
558 enhancement measured on the flight. (c) Altitude plot of example back trajectories showing coincident overshooting
559 (red squares). The green markers are overshooting convective tops within +/-3 hours of the red squares. The high
560 resolution of the convective overshooting data meant that there could be multiple coincident convective
561 overshooting cells for a single location on a back trajectory, (d) Days between OT and intercept by aircraft on 8
562 August 2013.
563
564 **Figure 7.** Analysis of the 16 August 2013 NASA ER-2 flight. (a) Vertical profiles of JLH Mark2 *in situ* H_2O similar
565 to Figure 6a, (b) Back trajectories from the aircraft path similar to Figure 6b, (c) Altitude plot of back trajectories
566 showing coincident overshooting (red) and all overshooting within +/- 3 hours (green) similar to Figure 6c, (d) Days
567 between OT and intercept by aircraft similar to Figure 6d.
568
569 **Figure 8.** Analysis of the 27 August 2013 NASA ER-2 flight. (a) Vertical profiles of JLH Mark2 *in situ* H_2O similar
570 to Figure 6a, (b) Back trajectories from the aircraft path similar to Figure 6b, (c) Altitude plot of back trajectories
571 showing coincident overshooting (red) and all overshooting within +/- 3 hours (green) similar to Figure 6c, (d) Days
572 between OT and intercept by aircraft similar to Figure 6d.
573

574 **Figure 9.** Fraction of back trajectories that intersected OTs during the 7 previous days for the three SEAC^{4}RS flights
575 of 8 August (blue), 16 August (green) and 27 August 2013 (red) shown in Figures 6, 7 and 8, respectively.

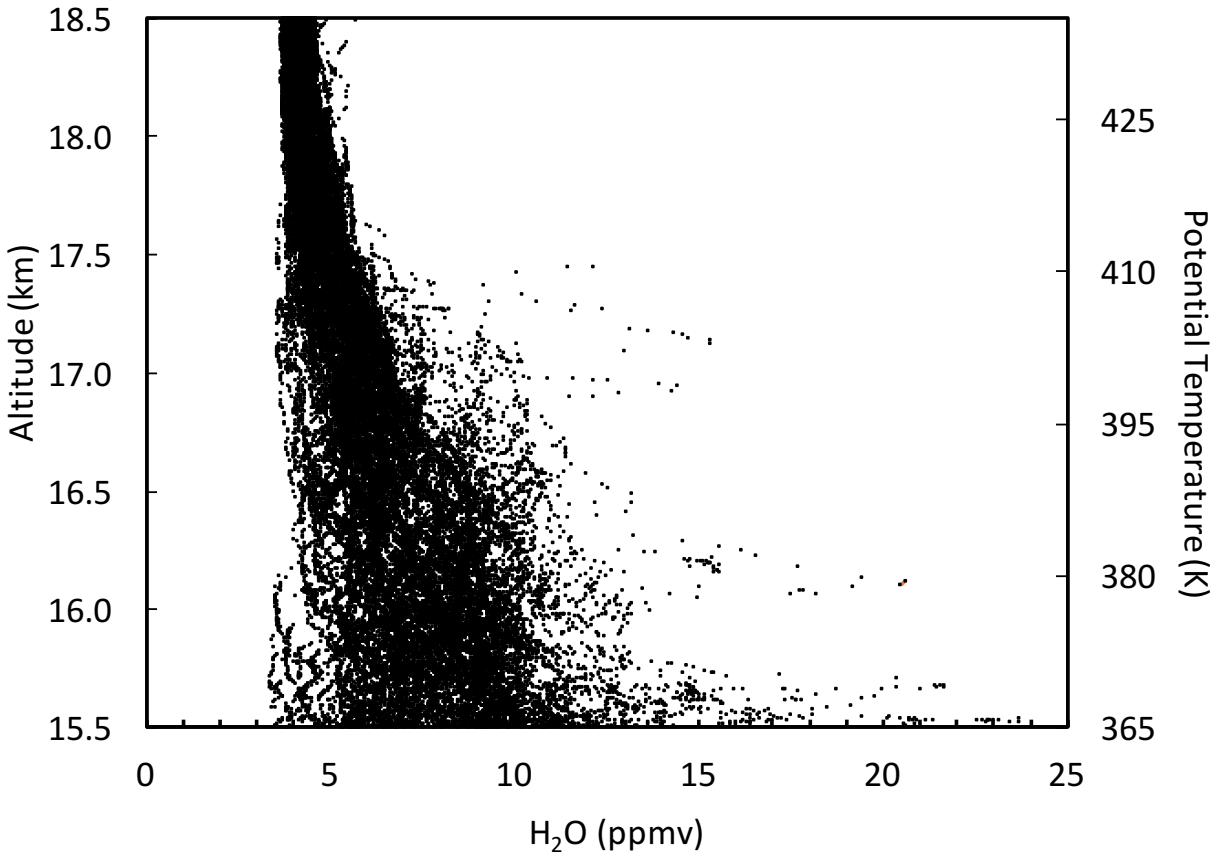

Figure 1. JLH Mark2 stratospheric water vapor profiles from 23 aircraft flights during SEAC^{4}RS. This altitude range includes the overworld stratosphere (potential temperature greater than 380 K) and lowermost stratosphere (tropopause to 380 K). The majority of observations have mixing ratios less than 10 ppmv in the lowermost stratosphere and less than 6 ppmv in the overworld stratosphere. Enhanced water measurements are the extreme outliers with high water mixing ratios, with a threshold value of mean plus two standard deviations.

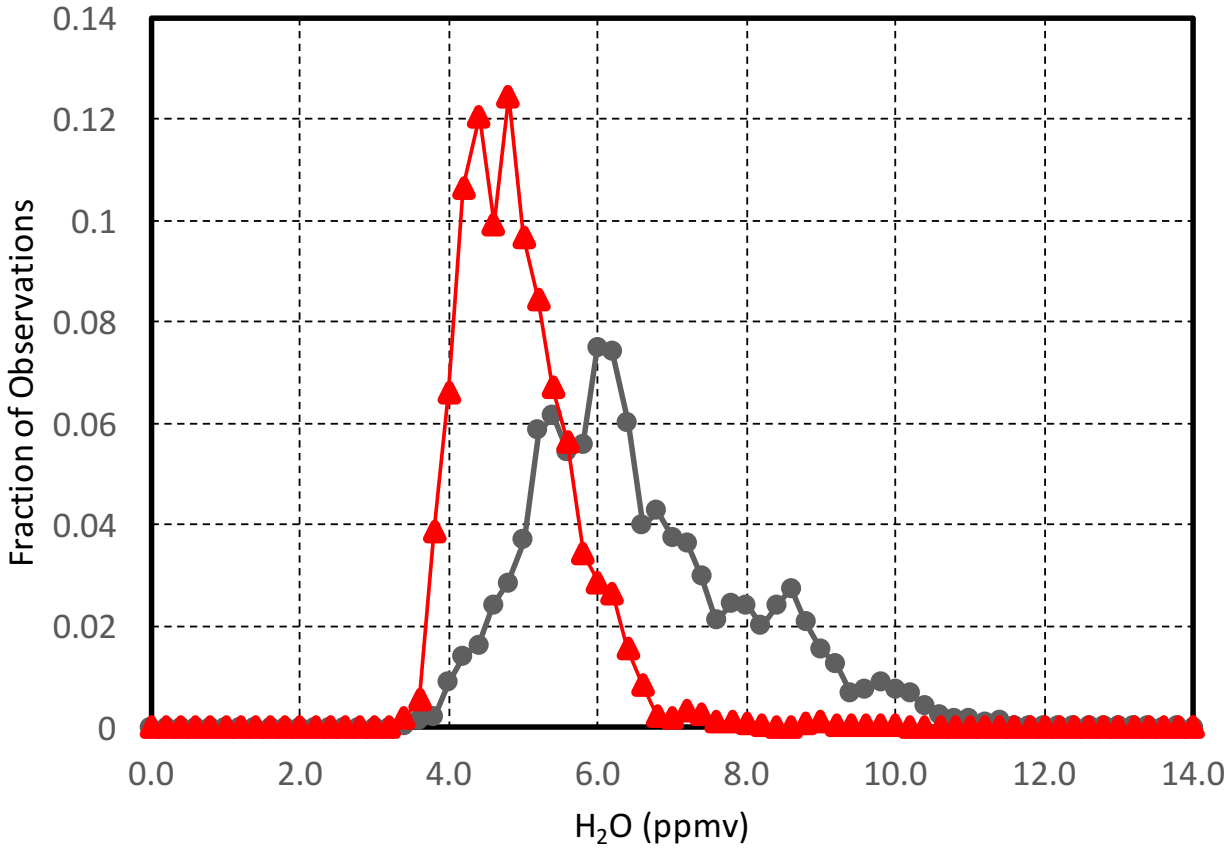

Figure 2. Distribution of JLH Mark2 water vapor in the overworld stratosphere for all flights in the SEAC^{4}RS mission (summer 2013), plotted as fraction of observations in each potential temperature range. First trace (black circles and line) is at potential temperatures 380 K to 400 K corresponding to approximately 16.8 to 17.4 km altitude (99 to 90 hPa). Second trace (red triangles and line) is at potential temperatures 400 to 420 K corresponding to approximately 17.4 to 18.0 km altitude (90 to 80 hPa).

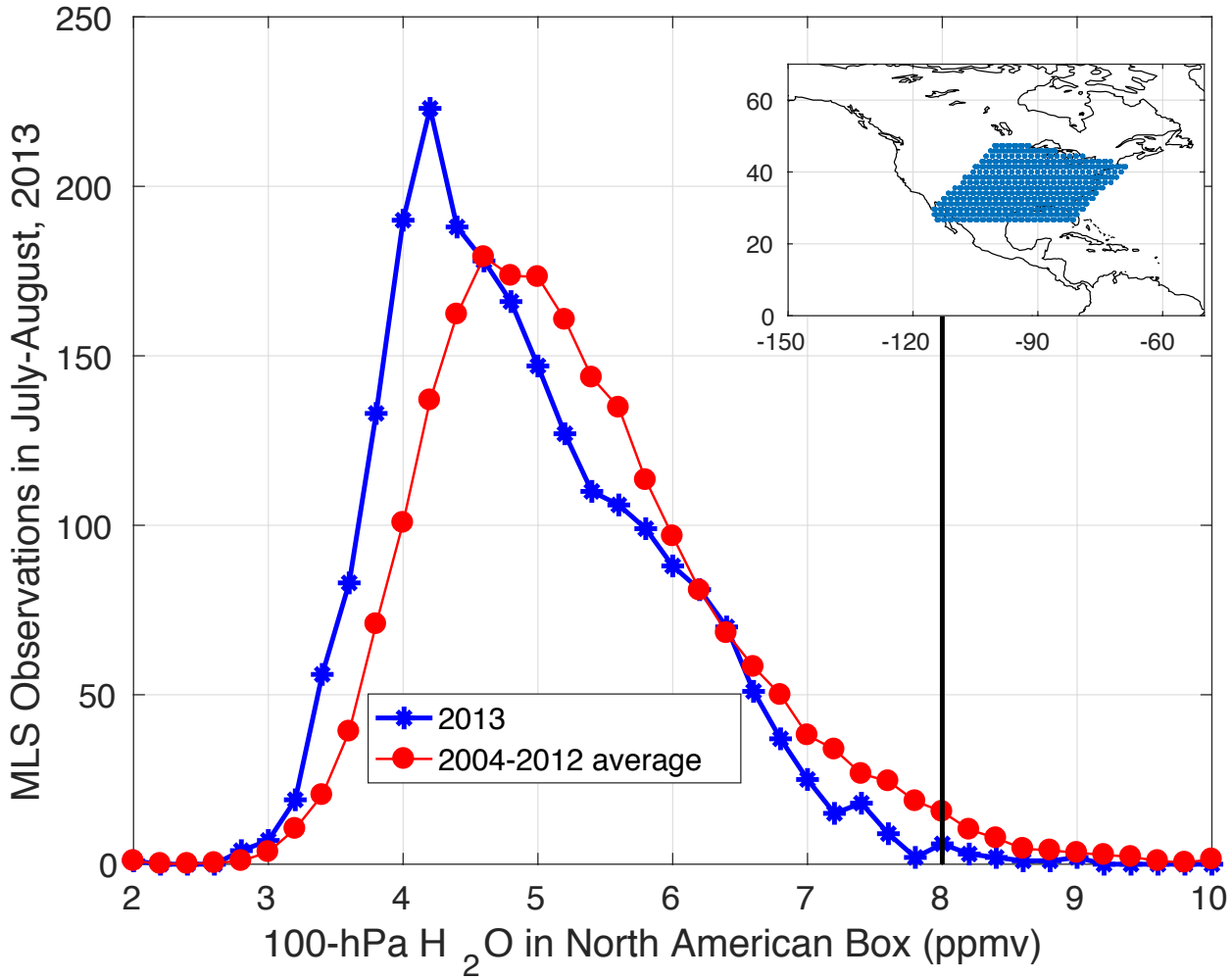

Figure 3. Distribution of Aura MLS v4.2 100-hPa H_2O over CONUS (blue shaded box in insert), corresponding to approximately 17 km altitude. The two histograms for July-August 2013 (blue asterisks and trace) and the previous nine-summer MLS record, July-August 2004 through 2012 (red circles and trace) indicates that 2013 was drier than average. The threshold for MLS-detected 'enhanced water vapor' (thick black vertical line) is set at 8 ppmv, same as Schwartz et al. (2013), to exclude the larger population of measurements at 6 to 8 ppmv water vapor that may have other sources.

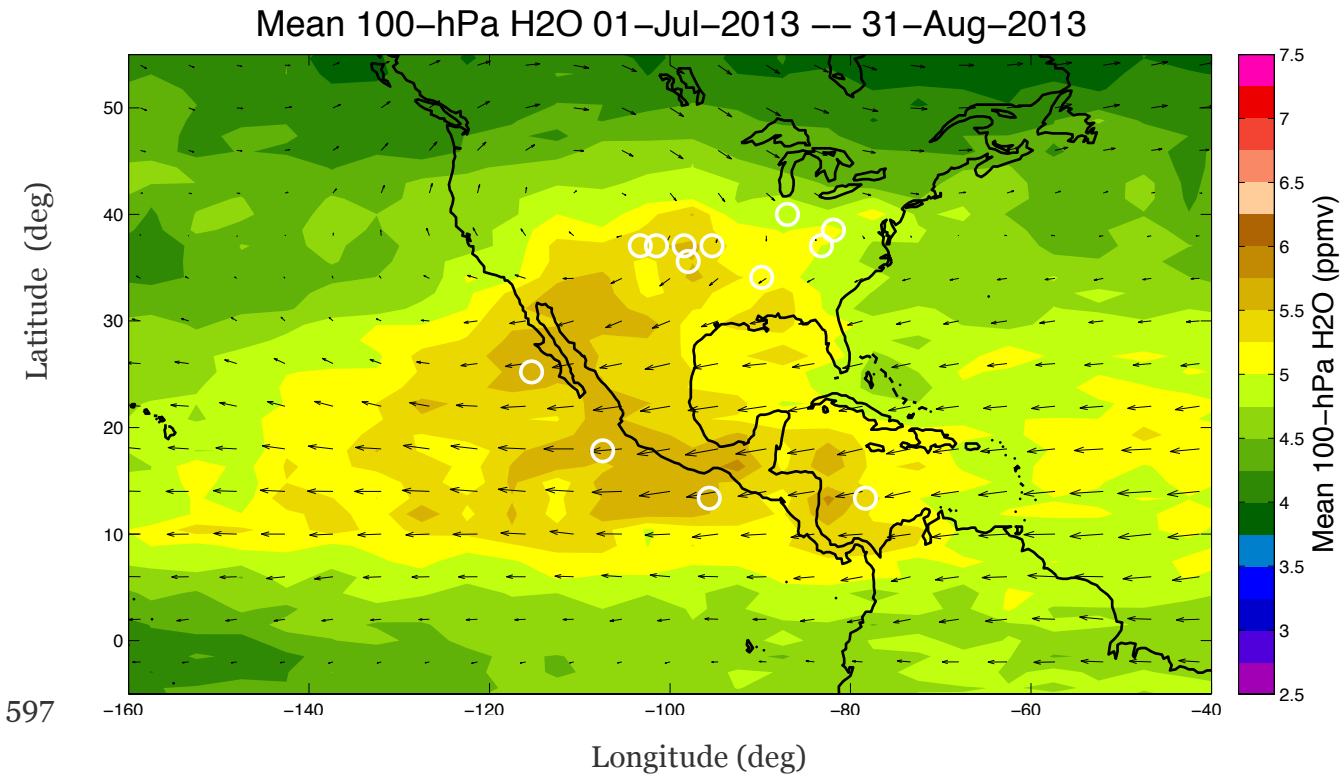

597

598 **Figure 4.** Two-month mean map of Aura MLS v4.2 100-hPa H_2O (color scale), corresponding to approximately 17
599 km altitude, with superimposed MERRA horizontal winds (arrows) for July-August 2013 during the SEAC^{4}RS time
600 period. MLS observations of 100-hPa H_2O greater than 8 ppmv in this two-month period are shown by the white
601 circles.

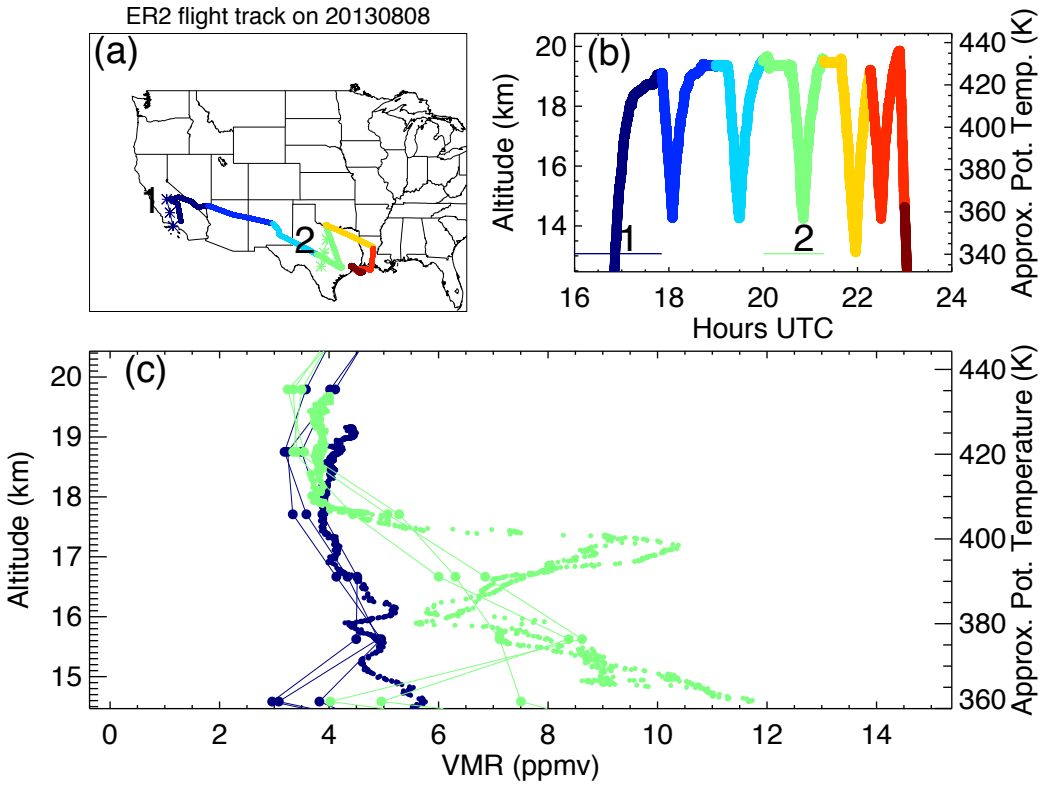

Figure 5. Map and profiles of aircraft and satellite water vapor on 8 August 2013 over California (number 1 shown in dark blue) and Texas (number 2 shown in green). (a) Map of ER-2 aircraft flight track (solid colored trace) and nearly coincident Aura MLS geolocations (asterisks and lines). (b) ER-2 aircraft altitude profiles (solid colored trace) color-coded by dives and MLS times (horizontal lines). (c) Vertical profiles of *in situ* water vapor measurements from JLH Mark2 (dots) and MLS retrievals of water vapor (circles and lines). Some measurements exceed the threshold for enhanced water vapor of 8 ppmv for Aura MLS (after Schwartz et al., 2013), and the campaign-wide mean plus 2 st. dev. for JLH Mark 2, 9.7 ppmv at 380-400 K and 6.6 ppmv at 400-420 K.

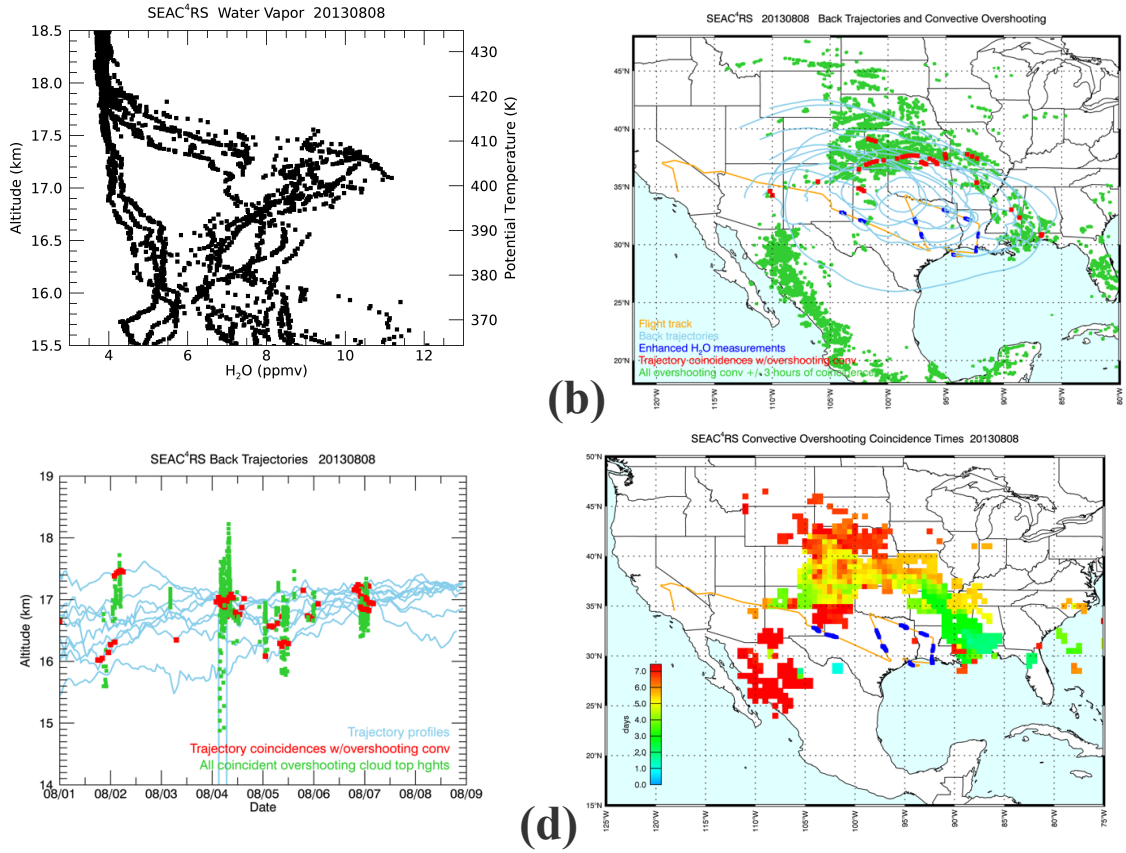

Figure 6. Analysis of the 8 August 2013 NASA ER-2 aircraft flight. (a) Vertical profiles of JLH Mark2 *in situ* H_2O. Back trajectories were initialized from all aircraft water measurements at 16 to 17.5 km altitude. (b) Example back trajectories (thin blue traces) and coincident overshooting convection (red). Along the NASA ER-2 flight track (orange line), enhanced water vapor was measured (thick blue lines). This figure identifies where trajectories and OT are coincident (red squares) within tolerances prescribed in Section 3.2. The green markers are overshooting convective tops within +/-3 hours of the red squares to indicate the main regions of convective overshooting during the seven days prior to the ER-2 flight and which of those regions appeared to contribute most to the water vapor enhancement measured on the flight. (c) Altitude plot of example back trajectories showing coincident overshooting (red squares). The green markers are overshooting convective tops within +/-3 hours of the red squares. The high resolution of the convective overshooting data meant that there could be multiple coincident convective overshooting cells for a single location on a back trajectory, (d) Days between OT and intercept by aircraft on 8 August 2013.

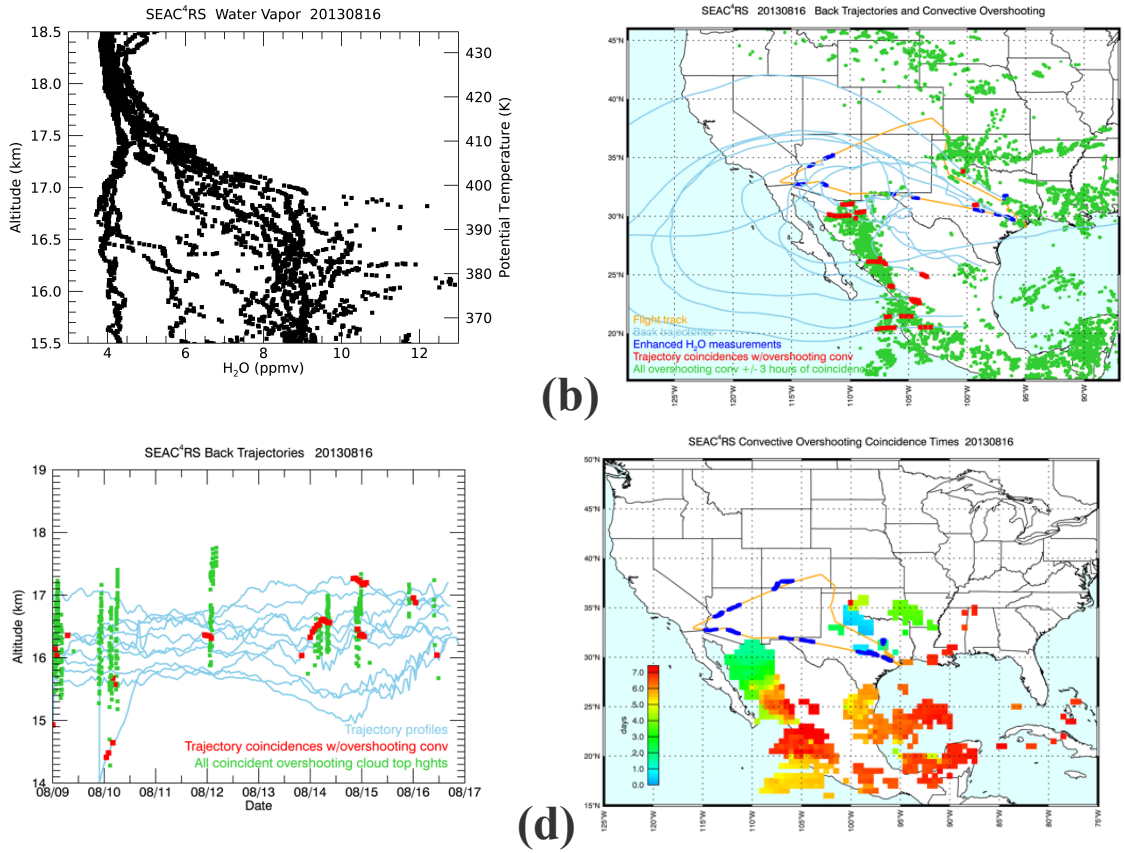

Figure 7. Analysis of the 16 August 2013 NASA ER-2 flight. (a) Vertical profiles of JLH Mark2 *in situ* H_2O similar to Figure 6a, (b) Back trajectories from the aircraft path similar to Figure 6b, (c) Altitude plot of back trajectories showing coincident overshooting (red) and all overshooting within +/- 3 hours (green) similar to Figure 6c, (d) Days between OT and intercept by aircraft similar to Figure 6d.

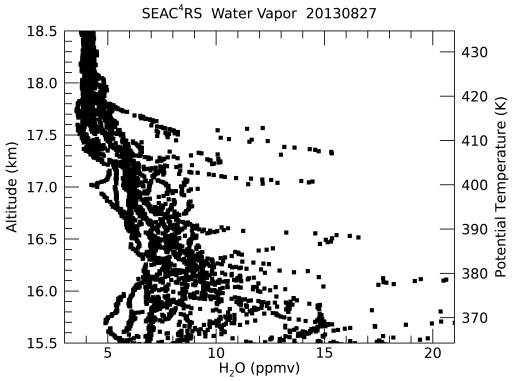

(a)

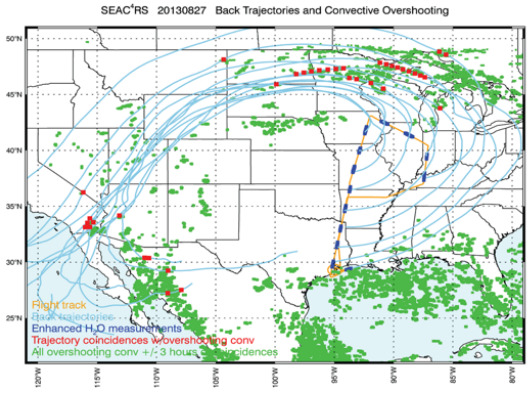

(b)

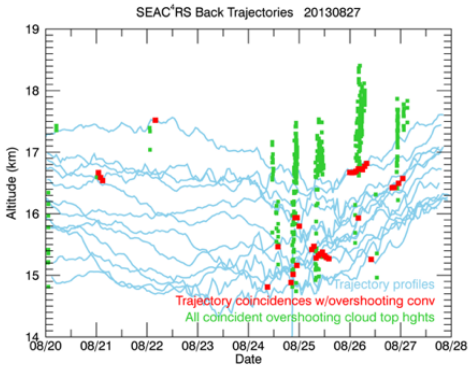

(c)

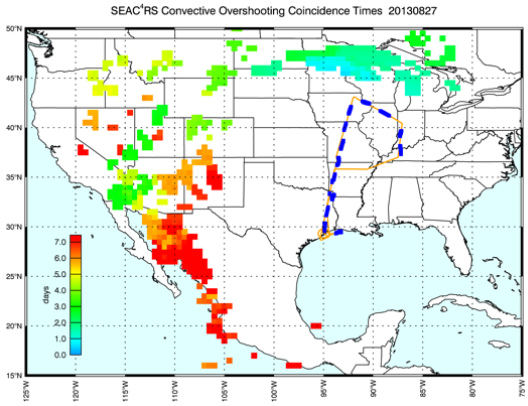

(d)

Figure 8. Analysis of the 27 August 2013 NASA ER-2 flight. (a) Vertical profiles of JLH Mark2 *in situ* H_2O similar to Figure 6a, (b) Back trajectories from the aircraft path similar to Figure 6b, (c) Altitude plot of back trajectories showing coincident overshooting (red) and and all overshooting within +/- 3 hours (green) similar to Figure 6c, (d) Days between OT and intercept by aircraft similar to Figure 6d.

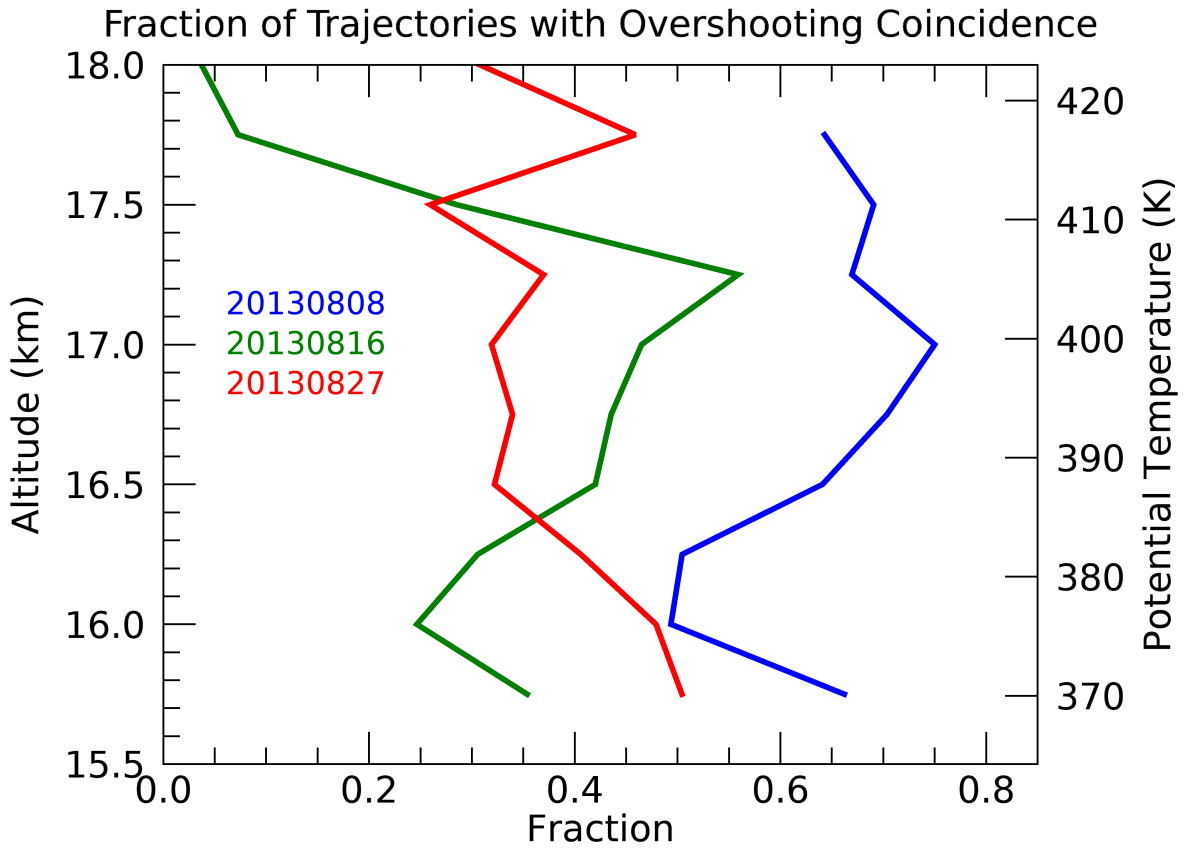

641

642 **Figure 9.** Fraction of back trajectories that intersected OTs during the 7 previous days for the three SEAC^{4}RS flights
643 of 8 August (blue), 16 August (green) and 27 August 2013 (red) shown in Figures 6, 7 and 8, respectively.